







Tunable in situ near-UV pulses by transient plasmonic resonance in nanocomposites

ANTON HUSAKOU,^{1,*}  IHAR BABUSHKIN,^{1,2,3}  OLGA FEDOTOVA,⁴  RYHOR RUSSETSKY,⁴ TATSIANA SMIRNOVA,⁵ OLEG KHASANOV,⁴ ALEXANDER FEDOTOV,⁵ USMAN SAPAEV,^{6,7}  AND TZVETA APOSTOLOVA^{8,9}

¹Max Born Institute, Max Born Str. 2a, 12489 Berlin, Germany

²Institute of Quantum Optics, Leibniz Hannover University, Welfengarten 1, 30167 Hannover, Germany

³Cluster of Excellence PhoenixD (Photonics, Optics, and Engineering – Innovation Across Disciplines), Welfengarten 1, 30167 Hannover, Germany

⁴Scientific and Practical Materials Research Center, Belarus NAS, Brovki 17, 220072 Minsk, Belarus

⁵Belarus State University, Niezaliežnasci Avenue 4, 220030 Minsk, Belarus

⁶Tashkent State Technical University, Universitet ko'chasi 2-uy, Almazar d/t, 100095 Tashkent, Uzbekistan

⁷Faculty of Technique, Urgench State University, Kh. Alimdjan Street 14, 220100 Urgench, Uzbekistan

⁸Institute for Nuclear Research and Nuclear Energy, Bulgarian Academy of Sciences, Tsarigradsko Chausse 72, 1784 Sofia, Bulgaria

⁹Institute for Advanced Physical Studies, New Bulgarian University, 1618 Sofia, Bulgaria

*gusakov@mbi-berlin.de

Abstract: We propose a concept for generation of ultrashort pulses based on transient field-induced plasmonic resonance in nanoparticle composites. Photoionization and free-carrier plasma generation change the susceptibility of nanoparticles on a few-femtosecond scale under the action of the pump pulse. This opens a narrow time window when the system is in plasmonic resonance, which is accompanied by a short burst of the local field. During this process, frequency-tunable few-fs pulses can be emitted. This paves a way to ultra-compact yet efficient generation of ultrashort pulses at short wavelengths.

© 2023 Optica Publishing Group under the terms of the [Optica Open Access Publishing Agreement](#)

1. Introduction

The ultrafast femtosecond-scale characterization and control of bound-electron motion [1] allow the measurement of solid-state properties [2] and is the key component of novel petahertz electronics. In particular, sufficiently strong pump pulses lead to a reversible transition of a material from insulator to conductor within one optical cycle [3]. Control of currents in solid state [4] and ultrafast metallization yield dramatic change of the material properties [5] that can be used for optical switching, signal processing etc. on the petahertz time scale. On the other hand, perspectives of short optical pulse generation offered by this ultrafast dynamics were barely investigated up to now.

Numerous fields of modern ultrafast optics, such as tracing of atomic motion in molecules [6], chemistry on electronic timescale [7], steering of ultrafast electron dynamics in the valence band [8], material modification [9] and so on, require short, sub-10-fs intense pulses at ultraviolet (UV) or near-UV frequencies. In the visible and near infrared ranges, ultrashort pulses are routinely generated using different approaches: directly from a laser oscillator [10], by a non-collinear optical parametric amplifier [11], or by spectral broadening in a nonlinear medium [12]. The extension of these techniques to the UV range is challenging due to the lack of broadband laser gain media in the UV (except for excimers of noble gas halides [13]) and strong two-photon absorption for high-energy photons [14] required for UV optical parametric amplifiers. For these

reasons, broadband UV pulses are typically generated in a two-step approach: first, few-optical-cycle pulses in the visible or near-infrared ranges are generated, and then nonlinear frequency up-conversion is used to reach the UV range. For frequency up-conversion in gases, the usually used nonlinear processes are third- or higher- order harmonic generation or four-wave-mixing between the fundamental wavelength and the second harmonic of the driving pulse, which is typically obtained from a Ti:sapphire laser. For example, sub-4-fs pulses at 270 nm were generated in Ne from the 6-fs laser output spectrally broadened in a hollow-core fiber [15], and 1.9-fs third-harmonic pulses with spectra from 210 to 340 nm were generated in argon gas cell [16]. UV pulses were also generated by second-order nonlinear frequency conversion in crystals, typically β -barium borate. For example, sub-10 fs 400 nm pulses were reported [17], and UV pulses with 9.7 fs pulse duration were generated by second harmonic generation using a spectrally shaped 1.9 mJ, 8 fs few-cycle near-infrared pulses [18]. Some new trends in the generation of UV pulses include dispersive-wave generation during the soliton propagation which provides an easy tunability over the entire ultraviolet and visible spectrum [19,20].

Due to a persistently high demand for short pulses in near-UV range and adjacent visible frequencies, it is promising and timely to search for alternative approaches to their generation, preferably directly from relatively long infrared pulses without compression step. Here, we seek to combine the two above-mentioned fields, and to utilize the perspectives offered by ultrafast carrier excitation and metallization of solids for the needs of ultrashort near-UV pulse generation.

A possibility to generate short UV pulses by a very small device in situ would be an important and highly desirable feature, particularly in view of biological applications. Indeed, during propagation in any transparent condensed matter, a ~ 10 -fs pulse will very quickly, on the sub-mm scale, become much longer due to group-velocity dispersion. Pre-compensation of group-velocity dispersion is in principle possible but challenging and requires precise a priori knowledge of the material properties, which is rarely available. Therefore it would be highly valuable to suggest a technique which allows generation of short pulses directly inside a transparent material at the desired position. On top of that, spectral tunability of the pulses would strongly enhance their application potential, e.g. by allowing to address different optical transitions.

In this paper we propose a method to generate such ultrashort tunable pulses using strongly nonlinear dynamics in a nanoparticle (NP) composite. The key idea of the paper is illustrated in Fig. 1. The incident long near-ir pulse, shown by the green curve, leads to transition of electrons from valence band to the first and higher conduction band (photoionization) inside the dielectric nanostructure. The motion of conduction-band electrons (plasma) is almost free, possibly with a modified effective mass. Therefore they provide a negative Drude-type contribution to the dielectric function of the NPs $\epsilon_i(t)$, which depends on time due to growing density of carriers ρ (illustrated by blue curve in Fig. 1). This process transiently converts a dielectric NP into a metallic one. Metallic NP are known to have a plasmonic resonance, where the local field is significantly enhanced. For NPs much smaller than the wavelength, the frequency of this plasmonic resonance is determined by the condition $2\epsilon_h + \epsilon_i(t) = 0$, where ϵ_h is the dielectric function of host material. For $2\epsilon_h + \epsilon_i(-\infty) > 0$, the plasmonic resonance can be reached only for a short time range when the relative plasma density is close to a certain value ρ_{res} . In this time range, the local field inside the NPs, proportional to $1/[2\epsilon_h + \epsilon_i(t)]$, shows a burst as illustrated by the red curve in Fig. 1. As will be discussed later, this burst and associated nonlinear processes lead to generation of short pulses at new frequencies (above the frequency of the pump field). All of the above aims: short near-UV pulse generation directly from long IR pulses, generation in situ at the position on NPs, as well as spectral tunability, are met by this design.

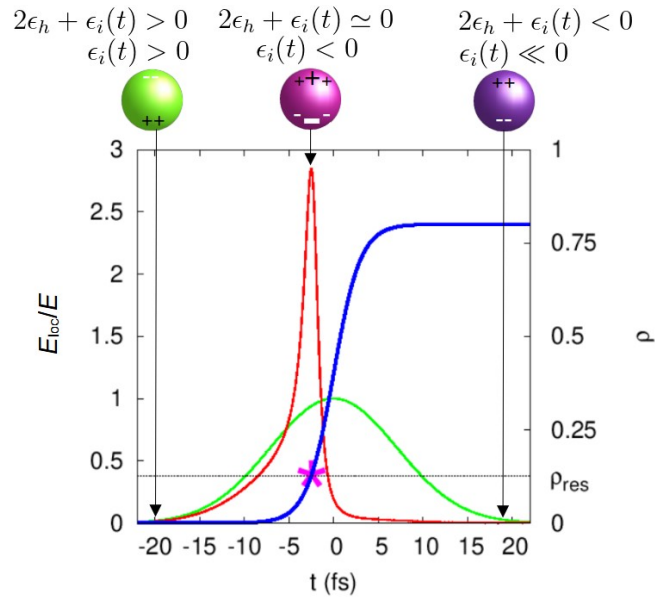


Fig. 1. The schematic representation of the key idea of the investigation. In a nanocomposite, the electric field inside the spherical nanoparticles (red curve) can be high compared to incident electric field (green curve) during the short time range when the plasmonic resonance (indicated by the magenta asterisk) is reached. The resonance takes place when the relative plasma density (blue curve) crosses the resonant value ρ_{res} indicated by the dashed black curve. In the top part of the figure the sign of the denominator $2\epsilon_h + \epsilon_i(t)$ which determines the plasmonic resonance, as well as the sign of the dielectric function $\epsilon_i(t)$ of the NPs, are indicated. On the surface of nanoparticles, charge distribution is schematically shown in each case.

2. Theoretical model

We consider a composite consisting of a homogeneous host material and spherical NPs with diameter well below the light wavelength so that effective-medium theory can be applied. A unidirectional (1+1)D propagation equation [21,22] is the most suitable for this kind of situations, since backward-propagating wave can be neglected. For details related to the propagation equation and the numerical procedure, see Ref. [23], Supplement 1.

The key equation describing the transient resonance is given by the ratio of the local field inside the nanoparticles E_{loc} , and the volume-averaged electric field E_{av} :

$$\frac{E_{\text{loc}}}{E_{\text{av}}} = \frac{3\epsilon_h}{2\epsilon_h + \epsilon_i(-\infty) - \frac{N\rho(t)e^2}{\epsilon_0 m_e \omega(\omega + i\nu)}}, \quad (1)$$

where N is the density of atoms/molecules in the NPs, $\rho(t)$ is the relative plasma density, and ν is the decay rate for the plasma motion. One can directly see the emergence of a transient plasmonic resonance for an appropriate value of $N\rho(t)$, when the denominator becomes close to zero. This equation provides self-consistent description of the local field E_{loc} in relation to averaged field E_{av} for any pump pulse and time-dependent plasma density. Here we note that we consider perfectly spherical NPs, however, for typical deviations of the shape from spherical the shift of the plasmonic resonance is relatively small, as discussed in detail in section 6 of Supplement 1.

Using a formal substitution $\omega \rightarrow i\partial_t$, we get

$$\left[\frac{\partial^2}{\partial t^2} + \nu \frac{\partial}{\partial t} \right] E_{\text{loc}}(t) = \kappa \rho(t) E_{\text{loc}}(t) + \frac{3\epsilon_h}{2\epsilon_h + \epsilon_i(-\infty)} \left[\frac{\partial^2}{\partial t^2} + \nu \frac{\partial}{\partial t} \right] E_{\text{av}}(t), \quad (2)$$

$$\frac{\partial \rho(t)}{\partial t} = \Gamma(E_{\text{loc}}(t)), \quad (3)$$

where $\kappa = \frac{Ne^2}{\epsilon_0 m_e}$. This system of equations allows rigorous description of transient plasmonic resonance and is the key novel contribution of our model. It allows to calculate the time-dependent ratio E_{loc}/E including the contribution of plasma.

Due to the high relevance of the photoionization for the considered process, it is critically important to develop an accurate formalism for the ionization rate in agreement with the experiment. After careful considerations based on the available experimental data as well as on our first-principle calculations of the ionization rate based on the numerical solution of the time-dependent 3D Schrodinger equation in single active electron approximation, we have found that ADK [24] ionization rate is the most suitable for our purposes, with corresponding material-dependent prefactors, as detailed in [Supplement 1](#).

Additionally, the following effects are taken into account: linear group velocity dispersion, intrinsic and scattering losses, third-order optical nonlinearities, as well as photoionization losses. For the derivation and details see [Supplement 1](#).

3. Numerical results

In Fig. 2, the numerical results for 25-fs, 25 TW/cm² pump pulses with 800 nm central wavelength, propagating in a composite of AlN particles (volume filling fraction $f = 0.003$) in SiO₂ host are presented. AlN and SiO₂ were chosen because of the relatively high damage thresholds (DT), broadband transmission, and availability for experimentalists. We have used available Sellmeyer-type expressions to model the dispersion of both materials [25,26], phenomenological values of the nonlinear susceptibilities [27–29], and the bandgap of 6.01 eV for the AlN [30]. Note that the fluence of above pulses is below the DT for fused silica of 1 J/cm², suggesting that ionization will be predominantly happening in the AlN NPs. We note parenthetically that absence or presence of backreflection is determined by *effective* refractive index, therefore for AlN NP composite (as opposed to bulk AlN) due to low filling factor f even significant levels of relative ionization in NPs will not lead to backreflection, and damage can be avoided even for $\rho \sim 1$.

From blue curves in left column in Fig. 2, one can see that indeed high levels of relative ionization are reached during the driving pulse. Slightly before the maximum of the pulse, the system passes through a plasmonic resonance, which manifests itself as a sharp peak of the field inside the NPs E_{loc} (red curve) as compared to the average field E_{av} (green curve). At the later stages of propagation, the input pulse is modified and depleted in the center of the pulse due to photoionization, as can be seen in Fig. 2(g). In the spectral domain, at the initial stage of the propagation a pronounced peak is formed at roughly (but not exactly) double the input frequency ω_0 , which later broadens and extends to higher frequencies. In the right column of Fig. 2, we show the temporal profile corresponding to this higher-frequency spectral components, by leaving only the spectral range from $1.2\omega_0$ to $3.5\omega_0$. It is important to note that we do not calculate the Fourier-limited pulse, rather, all the spectral phases which result from propagation are preserved. One can see that after only 35 nm of propagation, a well-isolated short pulse with a FWHM duration of 1.9 fs and weak pedestal is formed, with energy efficiency of 1.2% (corresponding to the efficiency determined from the peak field ratio of roughly 14%). Subsequent propagation, as illustrated in Fig. 2(i), shows further efficiency increase, which is however accompanied by longer and less regular pulse shape.

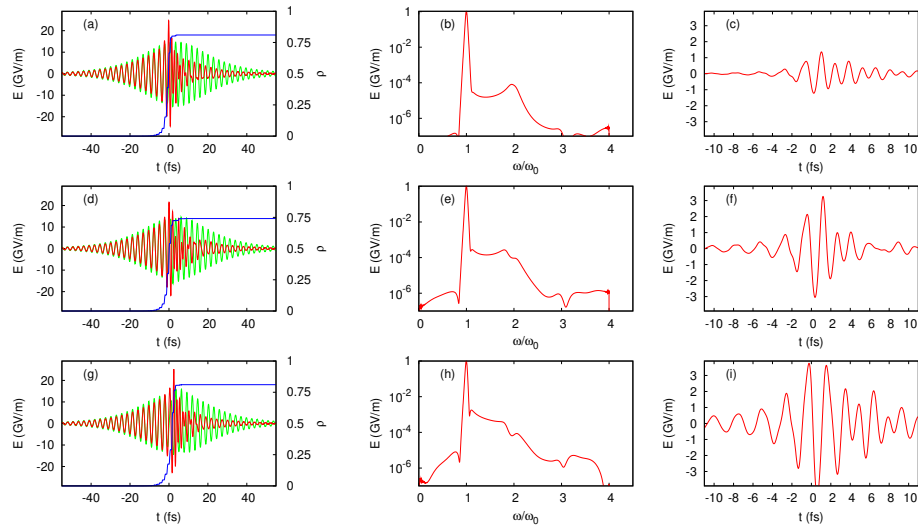


Fig. 2. The temporal properties [left column, (a),(d),(g)], spectra of the average field E_{av} [middle column, (b),(e),(h)], and temporal profiles generated short pulses [right column, (c),(f),(i)] for propagation distances of 15 nm [top row, (a),(b),(c)], 45 nm [middle row, (d),(e),(f)], 105 nm [bottom row, (g),(h),(i)]. Input pulse centered at 800 nm has a duration of 25 fs and intensity of 25 TW/cm². A composite of AlN NPs with identical radius of 2.5 nm and filling factor of $f = 0.003$ in SiO₂ host is considered. In left column, composite-averaged electric field (green curve), local field inside the NPs (red curve), and relative plasma density (blue curve) are shown.

4. Pulse tunability and generation mechanism

We explored the possibility to influence the position of the spectral peak visible in Fig. 2(b) by varying the pump pulse intensity and, correspondingly, the relative density of plasma after the pulse, $\rho(+\infty)$. In Fig. 3(a) we show that for different pump intensities it is possible to shift the peak (and the corresponding short pulse) in a significant spectral range, from 410 to 545 nm. The pulse duration varies slightly with intensity (not shown), but does not exceed 2.5 fs. In Fig. 3(b), the maximum wavelength of the peak is presented as a function of the relative density of plasma after the pulse, $\rho(+\infty)$.

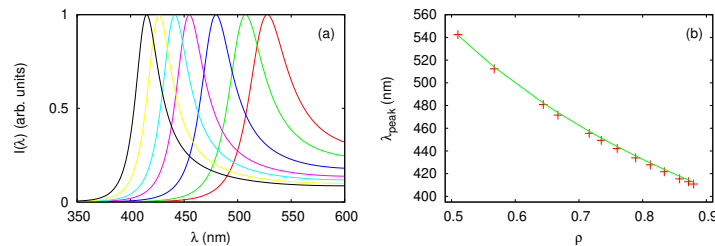


Fig. 3. Spectra of generated short pulse for different intensities (a) and the dependence of the central wavelength on the after-pulse plasma density (b). In (a), the intensities of 15.045 TW/cm², 15.05 TW/cm², 15.075 TW/cm², 15.2 TW/cm², 15.5 TW/cm², 17 TW/cm², 25 TW/cm² (from right to left) are considered. In (b), by solid green curve the analytical dependence given by Eq. (4) is shown.

The mechanism responsible for the generation of this peak is highly relevant to understand its tunability and further features. We note that it cannot be explained by the well-known plasma-induced blue shift of the spectrum, since such shift is proportional to the nonlinear phase accumulated during propagation, and therefore the position of the peak would be z -dependent, in contradiction to the numerical findings. Also, the energy of the peak grows quadratically with propagation length, which excludes amplification-like processes. Rather, we speculate that a short burst at the plasmonic resonance contains many spectral components. After the plasmonic resonance, the relative plasma density $\rho(+\infty) > \rho_{\text{res}}$ corresponds to the plasmonic resonance at frequency $\omega_* > \omega_0$. Spectral components at or around this frequency could be preserved and grow. To confirm this conjecture, in Fig. 3(b) we plot the wavelength corresponding to the resonant frequency after the pulse, the latter being given by

$$\omega_* = 0.91 \sqrt{\frac{Ne^2}{\epsilon_0 m_e [2\epsilon_h + \epsilon_i(+\infty)]}}. \quad (4)$$

In order to fit the numerical data, we have introduced a prefactor of 0.91, which is justified by the fact that the peak is generated under highly dynamical conditions with plasma density quickly changing in time. In Fig. 3(b), the prediction given by Eq. (4) is shown by the green curve. An almost perfect agreement with numerical results is obtained. Even with a fit parameter, such agreement is highly indicative that proposed mechanism indeed describes the peak generation in our system.

Note that the proposed mechanism allows *in situ* generation of short pulses. This can be achieved by simply placing the NPs (using e.g. optical nanotweezers technique [31] for NP manipulation, which is also available for biological matter [32]) at the desired position inside the material to be investigated, with this material simultaneously serving as a host medium for the proposed mechanism. Alternatively, for easily ionizable soft materials, one can place at a desired position a nanoscale piece of AlN-SiO₂ composite, using one of the microfluidic particle manipulation methods [33] such as electrophoresis.

With the aim to investigate the influence of the material choice of the transient plasmonic resonance, in Fig. 4 we show the numerical results for the 55-fs, 10 TW/cm² pulses at 800 nm propagating in a composite of ZnO NPs (volume filling fraction $f = 0.0003$) in SiO₂ host. Similar to the case of AlN NPs, phenomenological bulk material parameters were used [34–37]. ZnO has a much lower bandgap of 3.37 eV, which has significant influence on the dynamics. The dependence of the ionization rate on the intensity is smoother and does not have a strongly pronounced threshold-like character. Therefore the growth of the relative ionization, as shown in Fig. 4(a), occurs slower, and the system spends a longer time in the plasmonic resonance, as can be seen from comparison of local field (red curve) and average field (green curve) in Fig. 4(a). Correspondingly, the generated pulse is longer with FWHM of 9.5 fs, whereas the efficiency of 1.3% is comparable to AlN case. Despite the quantitative differences to AlN case, the generation of the short pulse is based on the same mechanism, as can be seen from the spectrum in Fig. 4(c) showing clear isolated feature around $1.4\omega_0$. We would like to stress that, despite the different ionization dynamics, for ZnO NPs the Eq. (4) provides accurate estimation of the peak spectral position using the same fitting factor of 0.91. We conclude that short pulse generation is possible for composites with host bandgap larger than inclusion bandgap, however, the latter should not be below roughly 4 eV for photoionization to be threshold-like. In addition, pedestal-free and sufficiently strong input pulses (intensity above 10 TW/cm²) are required.

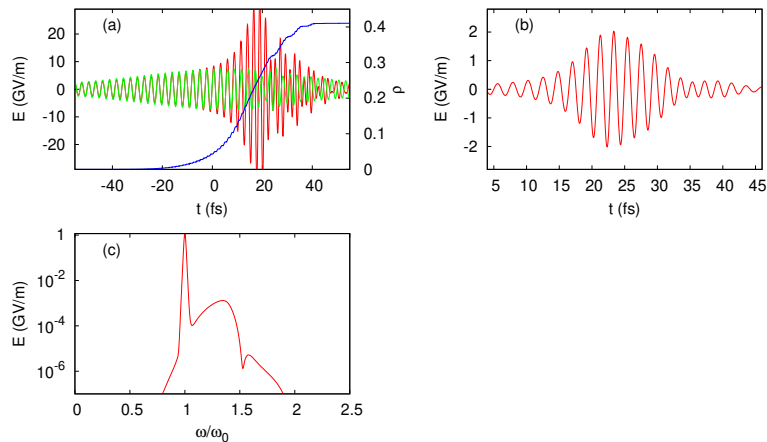


Fig. 4. The temporal properties (a), temporal profile of the generated short pulse (b), and spectrum (c) for propagation distance of 10 nm. Input pulse centered at 800 nm has a duration of 55 fs and intensity of 10 TW/cm^2 . A composite of ZnO NPs with identical radius of 2.5 nm and filling factor of 0.0003 in SiO_2 host is considered. In (a), composite-averaged electric field (green curve), local field inside the NPs (red curve), and relative plasma density (blue curve) are shown.

5. Conclusion

We have shown that strong optical field can lead to a transient metallization of a dielectric nanoparticle, forming a short burst of the local field inside the NPs as it crosses the plasmonic resonance. This process is accompanied by generation of tunable ultrashort light pulses at higher frequencies. For AlN and ZnO NPs, we predict a direct generation of tunable few-fs near-UV pulses from much longer near-IR pulses, with efficiencies reaching $\sim 1\%$ after only few tens of nanometers of propagation. We expect the proposed mechanism to be general and applicable beyond the examples considered here. As we have shown, it promises a new way to generate tunable, ultrashort radiation in nanosized devices, but it can be useful also in context of PHz-scale lightwave electronics [3,5].

Funding. Air Force Office of Scientific Research (FA8655-22-1-7175); European Research Executive Agency (H2020-MSCA-RISE-2018-823897); Cluster of Excellence PhoenixD (390833453); Bulgarian National Science Fund (KP-06-COST/7); World Bank Project (REP-04032022-206); Uzb-Ind (2021-96/83).

Disclosures. The authors declare no conflicts of interest.

Data availability. Data underlying the results presented in this paper are not publicly available at this time but may be obtained from the authors upon reasonable request.

Supplemental document. See [Supplement 1](#) for supporting content.

References

1. M. Hassan, T. Luu, A. Moulet, O. Raskazovskaya, P. Zhokhov, M. Garg, N. Karpowicz, A. M. Zheltikov, V. Pervak, F. Krausz, and E. Goulielmakis, "Optical attosecond pulses and tracking the nonlinear response of bound electrons," *Nature* **530**(7588), 66–70 (2016).
2. A. von Hoegen, R. Mankowsky, M. Fechner, M. Först, and A. Cavalleri, "Probing the interatomic potential of solids with strong-field nonlinear phononics," *Nature* **555**(7694), 79–82 (2018).
3. M. Schultze, E. M. Bothschafter, A. Sommer, S. Holzner, W. Schweinberger, M. Fiess, M. Hofstetter, R. Kienberger, V. Apalkov, V. S. Yakovlev, M. I. Stockman, and F. Krausz, "Controlling dielectrics with the electric field of light," *Nature* **493**(7430), 75–78 (2013).
4. V. Hanus, V. Csajbók, Z. Pápa, J. Budai, Z. Márton, G. Kiss, P. Sándor, P. Paul, A. Szeghalmi, Z. Wang, B. Bergues, M. Kling, G. Molnár, J. Volk, and P. Dombi, "Light-field-driven current control in solids with pJ-level laser pulses at 80-MHz repetition rate," *Optica* **8**(4), 570–576 (2021).

5. A. Schiffrin, T. Paasch-Colberg, N. Karpowicz, V. Apalkov, D. Gerster, S. Mühlbrandt, M. Korbman, J. Reichert, M. Schultze, S. Holzner, J. V. Barth, R. Kienberger, R. Ernstorfer, V. S. Yakovlev, M. I. Stockman, and F. Krausz, "Optical-field-induced current in dielectrics," *Nature* **493**(7430), 70–74 (2013).
6. A. Zewail, "Femtochemistry: Atomic-scale dynamics of the chemical bond," *J. Phys. Chem. A* **104**(24), 5660–5694 (2000).
7. F. Remacle and R. D. Levine, "An electronic timescale in chemistry," *Proc. Natl. Acad. Sci. U.S.A.* **103**(18), 6793–6798 (2006).
8. F. Remacle, M. Nest, and R. D. Levine, "Laser Steered Ultrafast Quantum Dynamics of Electrons in LiH," *Phys. Rev. Lett.* **99**(18), 183902 (2007).
9. T. Mocek, J. Polan, P. Homer, K. Jakubczka, B. Rus, I. J. Kim, C. M. Kim, G. H. Lee, C. H. Nam, V. Hajkova, J. Chalupsky, and L. Juha, "Surface modification of organic polymer by dual action of extreme ultraviolet/visible-near infrared ultrashort pulses," *J. Appl. Phys.* **105**(2), 026105 (2009).
10. R. Ell, U. Morgner, F. X. Kärtner, J. G. Fujimoto, E. P. Ippen, V. Scheuer, G. Angelow, T. Tschudi, M. J. Lederer, A. Boiko, and B. Luther-Davies, "Generation of 5-fs pulses and octave-spanning spectra directly from a Ti:sapphire laser," *Opt. Lett.* **26**(6), 373–375 (2001).
11. D. Brida, C. Manzoni, G. Cirmi, M. Marangoni, S. Bonora, P. Villoresi, S. De Silvestri, and G. Cerullo, "Few-optical-cycle pulses tunable from the visible to the mid-infrared by optical parametric amplifiers," *J. Opt.* **12**(1), 013001 (2010).
12. M. Nisoli, S. De Silvestri, O. Svelto, R. Szpocis, K. Ferencz, C. Spielmann, S. Sartania, and F. Krausz, "Compression of high-energy laser pulses below 5 fs," *Opt. Lett.* **22**(8), 522–524 (1997).
13. T. Nagy and P. Simon, "Generation of 200- μ J, sub-25-fs deep-UV pulses using a noble-gas-filled hollow fiber," *Opt. Lett.* **34**(15), 2300–2302 (2009).
14. P. Tzankov, T. Fiebig, and I. Buchvarov, "Tunable femtosecond pulses in the near-ultraviolet from ultrabroadband parametric amplification," *Appl. Phys. Lett.* **82**(4), 517–519 (2003).
15. U. Graf, M. Fiess, M. Schultze, R. Kienberger, F. Krausz, and E. Goulielmakis, "Intense few-cycle light pulses in the deep ultraviolet," *Opt. Express* **16**(23), 18956–18963 (2008).
16. M. Galli, V. Wanie, D. P. Lopes, E. P. Månsson, A. Trabattoni, L. Colaizzi, K. Saraswathula, A. Cartella, F. Frassetto, L. Poletto, F. L'Égaré, S. Stagira, M. Nisoli, R. M. Vázquez, R. Osellame, and F. Calegari, "Generation of deep ultraviolet sub-2-fs pulses," *Opt. Lett.* **44**(6), 1308–1310 (2019).
17. R. B. Varillas, A. Candeo, D. Viola, M. Garavelli, S. De Silvestri, G. Cerullo, and C. Manzoni, "Microjoule-level, tunable sub-10 fs by broadband sum-frequency generation," *Opt. Lett.* **39**(13), 3849–3851 (2014).
18. F. Xiao, X. H. Fan, L. Wang, D. W. Zhang, J. H. Wu, X. Wang, and Z. X. Wand Zhao, "Generation of Intense Sub-10-fs Pulses at 385 nm," *Chin. Phys. Lett.* **37**(11), 114202 (2020).
19. C. Brahms, F. Belli, and J. C. Travers, "Infrared attosecond field transients and UV to IR few-femtosecond pulses generated by high-energy soliton self-compression," *Phys. Rev. Res.* **2**(4), 043037 (2020).
20. A. Lekosiotis, C. Brahms, F. Belli, T. F. Grigoroza, and J. C. Travers, "Ultrafast circularly polarized pulses tunable from the vacuum to deep ultraviolet," *Opt. Lett.* **46**(16), 4057–4059 (2021).
21. A. Husakou and J. Herrmann, "Supercontinuum Generation of Higher-Order Solitons by Fission in Photonic Crystal Fibers," *Phys. Rev. Lett.* **87**(20), 203901 (2001).
22. J. C. Maxwell Garnett, "Colours in Metal Glasses and in Metallic Films," *Philos. Trans. R. Soc. London* **203**(359-371), 385–420 (1904).
23. A. Husakou, I. Babushkin, O. Fedotova, R. Rysetsky, T. Smirnova, O. Khasanov, A. Fedotov, U. Sapaev, and T. Apostolova, "Unified Model for Nonlinear Pulse Propagation in Composites and Optimization of THz Generation," *Phys. Rev. A* **108**(1), 013506 (2023).
24. M. V. Ammosov, N. B. Delone, and V. P. Krainov, "Tunnel ionization of complex atoms and atomic ions in an electromagnetic field," *Sov. Phys. JETP* **64**, 1191–1196 (1986).
25. J. Pastrnak and L. Roskocova, "Refraction index measurements on AlN single crystals," *Phys. Status Solidi B* **14**(1), K5–K8 (1966).
26. C. Z. Tan, "Determination of refractive index of silica glass for infrared wavelengths by IR spectroscopy," *J. Non-Cryst. Solids* **223**(1-2), 158–163 (1998).
27. W. H. P. Pernic, C. Xiong, C. Schuck, and H. X. Tang, "Second harmonic generation in phase matched aluminum nitride waveguides and micro-ring resonators," *Appl. Phys. Lett.* **100**(22), 223501 (2012).
28. H. Jung, C. Xiong, K. Y. Fong, X. Zhang, and H. X. Tang, "Optical frequency comb generation from aluminum nitride microring resonator," *Opt. Lett.* **38**(15), 2810–2812 (2013).
29. D. Milam, "Review and assessment of measured values of the nonlinear refractive-index coefficient of fused silica," *Appl. Opt.* **37**(3), 546–550 (1998).
30. M. Feneberg, R. A. R. Leute, B. Neuschl, K. Thonke, and M. Bickermann, "High-excitation and high-resolution photoluminescence spectra of bulk AlN," *Phys. Rev. B* **82**(7), 075208 (2010).
31. J. Berthelot, S. S. Acimovic, M. L. Juan, M. P. Kreuzer, J. Renger, and R. Quidant, "Three-dimensional manipulation with scanning near-field optical nanotweezers," *Nat. Nanotechnol.* **9**(4), 295–299 (2014).
32. Y.-C. Li, H.-B. Xin, H.-X. Lei, L.-L. Liu, Y.-Z. Li, Y. Zhang, and B.-J. Li, "Manipulation and detection of single nanoparticles and biomolecules by a photonic nanojet," *Light: Sci. Appl.* **5**(12), e16176 (2016).

33. S. Zhang, Y. Wang, P. Onck, and J. den Toonder, "A concise review of microfluidic particle manipulation methods," *Microfluid. Nanofluid.* **24**(4), 24–44 (2020).
34. I. Bodurov, I. Vlaeva, A. Viraneva, T. Yovcheva, and S. Sainov, "Modified design of a laser refractometer," *Nanoscience Nanotechnology* **16**, 31–33 (2016).
35. G. Wang, G. K. L. Wong, and J. B. Ketterson, "Redetermination of second-order susceptibility of zinc oxide single crystals," *Appl. Opt.* **40**(30), 5436–5438 (2001).
36. M. C. Larciprete, D. Haertle, A. Belardini, M. Bertolotti, F. Sarto, and P. Günter, "Characterization of second and third order optical nonlinearities of ZnO sputtered films," *Appl. Phys. B* **82**(3), 431–437 (2006).
37. V. V. Multian, J. Riporto, M. Urbain, Y. Mugnier, G. Djanta, S. Beauquis, C. Galez, V. Ya Gayvoronsky, and R. Le Dantec, "Averaged third-order susceptibility of ZnO nanocrystals from Third Harmonic Generation and Third Harmonic Scattering," *Opt. Mater.* **84**, 579–585 (2018).